

1 **Land subsidence in the Friuli Venezia Giulia coastal plain, Italy: 1992-2010 results**  
2 **from SAR-based interferometry**

3

4 Cristina Da Lio <sup>a</sup> and Luigi Tosi <sup>a,\*</sup>

5 <sup>a</sup>Institute of Marine Sciences, National Research Council,

6 Arsenale Tesa 104, Castello 2737/F, 30122 Venice, Italy

7

8 \* Corresponding author. Luigi Tosi, e-mail: [luigi.tosi@ismar.cnr.it](mailto:luigi.tosi@ismar.cnr.it), Institute of Marine  
9 Sciences, National Research Council, Arsenale Tesa 104, Castello 2737/F, 30122  
10 Venice, Italy.

11

12 **ABSTRACT**

13 Land subsidence is a concern in many coastal plains worldwide, particularly in the low-  
14 lying areas already facing sea level rise due to climate change, and much still needs to  
15 be done, with respect to both mapping land subsidence and gaining a comprehensive  
16 understanding of the relevant cause-effect relationships. Land subsidence of the  
17 northern coastal plain encompassing the Friuli Venezia Giulia (FVG) region in Italy,  
18 remains, to the authors' knowledge, poorly investigated. This coastland includes low-  
19 lying agricultural and urban areas and highly valuable lagoon environments,  
20 archaeological and touristic sites, and industrial zones.

21 Here, we resolve land subsidence in the coastal plain between the Tagliamento River  
22 delta and the Isonzo River mouth over the period 1992-2010 using Envisat ASAR and  
23 ERS1/2 interferometric datasets. **We identify a large variability of the land subsidence**  
24 **and a spatial gradient that ranges from less than 1 mm/yr in the high southwestern plain**

25 toward the littoral to more than 5 mm/yr close to the Tagliamento River delta. A  
26 comparison between the 2003-2010 and 1992-2000 sinking rates depicts quite similar  
27 behaviors of the process over the two time spans. The analysis indicates unclear  
28 correlations between ground movements and the typical driving mechanisms acting in  
29 the north Adriatic coastal plains, such as the variability of the morphological setting, the  
30 subsoil characteristics and the land use. We reason that multi-component mechanisms  
31 contribute to the observed image of the subsidence in the FVG coastland. Specifically,  
32 anthropogenic activities, e.g., groundwater exploitations, hydraulic reclamations and the  
33 development of newly built-up areas, are superposed to natural mechanisms related to  
34 the spatial variability of the subsoil characteristics, typical of transitional coastal  
35 environments.

36

37 **Keywords:** Land subsidence, Friuli Venezia Giulia coastland, Grado-Marano lagoon,  
38 SAR interferometry

39

## 40 **1. Introduction**

41 Coastal plains, river deltas, estuaries, tidal marshes and lagoons are the environments  
42 most susceptible to the effect of land subsidence worldwide because a key determinant  
43 of their vulnerability is the extent to which the lowering of their surface elevation  
44 contributes to relative sea level rise. Therefore, understanding subsidence-induced  
45 changes in these landscapes represents a breakthrough in sustainable land use, flood  
46 mitigation and restoration plans, safeguarding of natural and cultural heritages and the  
47 safety of people that live on them (Syvitski et al., 2009; Abidin et al., 2011).

48 The northwestern Adriatic coast encompasses the largest Mediterranean low-lying  
49 coastlands, including deltas, estuaries, lagoons, wetlands, and farmlands, whose present  
50 landscape is the result of hundreds of years of human intervention. Anthropogenic  
51 activities and urban and industrial centers threaten these valuable transitional  
52 ecosystems and historical and archaeological sites, which are found widely throughout  
53 the northern Adriatic coast.

54 The coast of the Friuli Venezia Giulia (FVG) region is located in the northernmost  
55 Italian tip facing the Adriatic Sea. The coast is characterized by a Pleistocene-Holocene  
56 plain sector, including the Grado-Marano lagoon, minor wetlands, the Tagliamento  
57 River delta and the Isonzo estuary, and a carbonate steep cliff sector related to the alpine  
58 chain.

59 Most of the coastal plain is characterized by low-lying parts that are below sea level and  
60 covered by farmlands and minor urban centers. These features are the results of  
61 hydraulic reclamation works carried out over the past centuries to drain former wetlands  
62 and lagoons.

63 Therefore, the preservation of ground elevation is one of the main issues facing this  
64 area, in addition to maintaining the efficiency of the drainage systems to reduce the  
65 effects of flooding and seawater intrusion (Da Lio et al., 2015). The Grado-Marano  
66 lagoon is an extremely important wetland of significant ecological worth that is  
67 particularly fragile (Fontolan et al., 2012). The morphology of the lagoon is a result of  
68 sedimentary processes (e.g., deposition, erosion), climate change (e.g., sea level rise,  
69 storms), and human interventions and activities (e.g., coastal protections, land use).  
70 Consequently, the lagoon ecosystem depends on the mutual interaction between these

71 forces, among which the effect of the relative sea level rise (RSLR), i.e., eustacy plus  
72 subsidence, must also be included (Carbognin and Tosi, 2002).

73 The study of land subsidence in the north Adriatic coastland dates back to the mid-  
74 1900s. Since then, hundreds of analyses have been performed. The Po River delta and  
75 the Veneto and Emilia Romagna coastal plains are the areas most commonly  
76 investigated, whereas the subsidence along the FVG coast remains poorly investigated.  
77 Marchesini et al. (2006) analyzed the displacements measured across different time  
78 spans over the period 1980-2004 along a local leveling network bounding the eastern  
79 part of the Grado-Marano lagoon and noted a general subsidence trend of approximately  
80 2 mm/yr and a local sinking rate of 3-4 mm/yr. Through a comprehensive investigation  
81 of the relative sea level changes of the Italian coastlines, Antonioli et al. (2009)  
82 analyzed the ground movements of national leveling lines and noted an increasing  
83 subsidence trend from both Venice and Trieste toward the Tagliamento River with  
84 sinking values ranging from 3 to 4 mm/yr in the nearby northern lagoon margin. Alfarè  
85 et al. (2014) using SAR-based interferometry and geological data to assess the  
86 subsidence in a restricted sector of the FVG coastland including the historical city of  
87 Aquileia and a small part of the Grado-Marano lagoon. The results of this study noted  
88 the significant heterogeneity of the subsidence process, which has never been assessed  
89 using leveling.

90 Presently, despite the high vulnerability of coasts to climate change hazards (e.g.,  
91 Torresan et al., 2012) and the need to protect the great environmental, agricultural and  
92 cultural value of the FVG coastland, a comprehensive and detailed assessment of the  
93 land subsidence characterizing this area has, to the authors' knowledge, never been  
94 conducted.

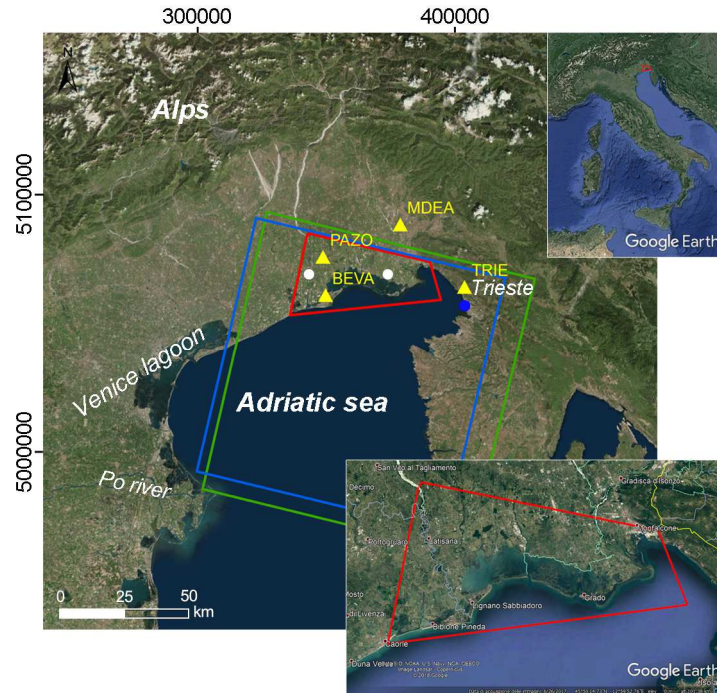
95 Starting in 2007, the Italian Ministry of the Environment and Protection of Land and  
96 Sea, within the framework of the Special Plan of Remote Sensing of the Environment,  
97 committed to measuring surface deformation using SAR-based interferometry of all  
98 available Envisat ASAR and ERS images over Italy. However, in many cases, the  
99 interferometric products are not directly usable for quantifying absolute ground  
100 velocities at regional scales because they are biased by arbitrary null movement point  
101 references and by flattening (Tosi et al., 2013; Tosi et al., 2015).

102 Here, we use these interferometric products to provide a comprehensive picture of the  
103 land subsidence in the FVG coastal plain (Fig. 1) and to highlight driving mechanisms  
104 acting at the regional and local scales related to natural processes and anthropogenic  
105 activities such as groundwater exploitation, hydraulic reclamation, agriculture and  
106 urbanization.

107 Specifically, we apply the post-processed de-flattening procedure described by Tosi et  
108 al. (2015) necessary to obtain land displacements at millimeter-scale accuracy in large  
109 areas, as already adopted in many subsidence studies of the Venice coastlands, e.g.,  
110 Teatini et al. (2012), Tosi et al. (2013), Tosi et al. (2016), and Da Lio et al. (2018). Such  
111 a procedure consists in implementing correction planes modeled through ground-based  
112 data to mitigate the slight phase tilt resulting by the imperfect knowledge of satellite  
113 positions.

114 This paper is organized as follows. First, the calibration and de-flattening of Envisat  
115 ASAR and ERS1/2 interferometric products using ground-based measurements is  
116 discussed. Second, an analysis of the distribution and temporal evolution of land  
117 subsidence is presented. Third, potential mechanisms driving subsidence are discussed

118 and, finally, the coastal subsidence of the FVG is compared with that of the adjacent  
119 areas of the northern Adriatic coastland.  
120



121  
122 **Fig. 1.** Satellite image of the northern Adriatic coastland. The study area is indicated by  
123 the red polygon. The footprints of ERS1/2 (Track 351 - Frame 2691) and Envisat ASAR  
124 (Track 351 - Frame 2691) frames are represented by blue and green boxes, respectively.  
125 Yellow triangles: positions of the CGPS stations; white dots: positions of the leveling  
126 benchmarks; blue dot: tide gauge station.

127

## 128 **2. Material and methods**

129 The analysis of land subsidence in the FVG coast is based on persistent scatterer  
130 interferometry (PSI) products obtained by Envisat ASAR and ERS1/2 images and made  
131 available by the National Geoportal of the Italian Ministry of the Environment and

132 Protection of Land and Sea (<http://www.pcn.minambiente.it/mattm/en/>). Specifically,  
133 we used the following datasets (Fig. 1):

134 - Envisat ASAR, Track 351 - Frame 2691, consisting of a stack of 37 descending  
135 stripmap images (C-band) acquired between 2003 and 2010 with a revisiting time of 35  
136 days, quite irregular in the study area, generally spanning from 35 and 70 days;

137 - ERS1/2 Track 351 - Frame 2691, consisting of a stack of 72 descending stripmap  
138 images (C-band) acquired between 1992 and 2000 with a revisiting time of 35 days and  
139 quite regular acquisition in the study area.

140 A detailed description of the interferometric processing of these datasets has been  
141 provided by Costantini et al. (2017).

142 The interferometric products refer to arbitrary null displacement reference points and  
143 are affected by slight tilting due to the imperfect knowledge of satellite orbits, both  
144 issues compromising the reliability of ground movements, particularly mapping at the  
145 regional scale. To reduce these biases, calibration and de-flattening were previously  
146 performed using correction planes modeled through ground-based data (Teatini et al.,  
147 2012; Tosi et al., 2015) by i) defining a local reference frame based on a reference point  
148 located outside the study area and the subsiding coastland and ii) projecting the vertical  
149 velocities of the ground-truth data along the line of sight (LOS) of the satellites (Da Lio  
150 et al., 2018).

151 Four permanent continuous GPS stations (CGPS) properly distributed in the monitored  
152 area were selected from the MAGNET GPS network (IGS08 datum, e.g., Rebischung et  
153 al., 2011) and used for calibration and de-flattening of the Envisat interferometric  
154 product (<http://geodesy.unr.edu>). Specifically, three of these CGPS stations are located  
155 inside the area covered by the interferometric dataset, i.e., PAZO in the northwestern

156 part, TRIE in the eastern part, and BEVA in the southernmost part close to the Grado-  
157 Marano lagoon and Tagliamento River; one, MDEA, lies just outside the SAR frames in  
158 the northern part of the study area and is used to refer the horizontal movements (Fig.  
159 1). The time intervals spanned by the selected CGPS match those spanned by the  
160 Envisat ASAR data, with the exception of BEVA CGPS, which is shorter and covers  
161 only the last two years of the 2003-2010 period. For this latter dataset, we assumed  
162 negligible change in the ground movement trend.

163 Because ERS1/2 images were acquired prior to the installation of the CGPS stations,  
164 leveling data from the Italian Military Geographic Institute - IGMI  
165 (<https://www.igmi.org/en>), the former hydrographic office of the Venice Water  
166 Authority - UIMA (<http://provveditoratovenezia.mit.gov.it/>), and the tide gauge station  
167 of Trieste (e.g., Carbognin et al., 2010) were used to calibrate the 1993-2000  
168 interferometric product (Fig. 1).

169

### 170 **3. Results**

#### 171 **3.1 Recent land subsidence over 2003-2010 period**

172 The interferometric solutions provided by the Special Plan of Remote Sensing of the  
173 Environment refer to arbitrary null movement points and are affected by the so-called  
174 flattening problem, i.e., the slight phase tilt resulting from the inaccuracy in estimating  
175 the orbital baseline due to the imperfect knowledge of satellite positions. Therefore, we  
176 adjusted the PSI solution with a correction plane model fitting the velocities of the three  
177 CGPS (<http://geodesy.unr.edu>) considered as ground truths (Table 1).

178 The CGPS horizontal land movements refer to a fourth CGPS station (MDEA CGPS;  
179  $13^{\circ} 26' 8.16''$  E,  $45^{\circ} 55' 28.20''$  N) located outside the study area. Because the horizontal



180 movements (N and E) of MDEA CGPS are assumed to be representative of the regional  
 181 plate motion, its average velocities in the N and E directions, i.e., 17.6 and 21.6 mm/yr,  
 182 respectively, were removed from all the other CGPS stations (Table 1). In addition,  
 183 considering that SAR interferometry provides land displacements along the line of sight  
 184 (LOS) between a satellite and the targets, the three-dimensional CGPS velocity vectors  
 185 must be projected onto the SAR LOS using Eq. (1):

$$186 \quad CGPS_{LOS} = \sin(\theta) \cos(\phi) \Delta E + \sin(\theta) \sin(\phi) \Delta N + \cos(\theta) UP \quad (1)$$

187  $\Delta E$  and  $\Delta N$  are the local easting and northing components of the CGPS, computed by  
 188 removing the E and N average velocities of MDEA, and UP is the vertical component.  
 189 The incidence angle,  $\theta$ , and the ground track angle,  $\phi$ , at the CGPS locations were  
 190 assumed to be equal to those of the frame, i.e.,  $22^\circ$  and  $5^\circ$ , respectively (SAR metadata  
 191 available from the Italian Ministry of the Environment and Protection of Land and Sea).

192

193 **Table 1.** Position, easting (E), northing (N), vertical (UP), and LOS velocities of the  
 194 CGPS stations used for the calibration of the SAR dataset.

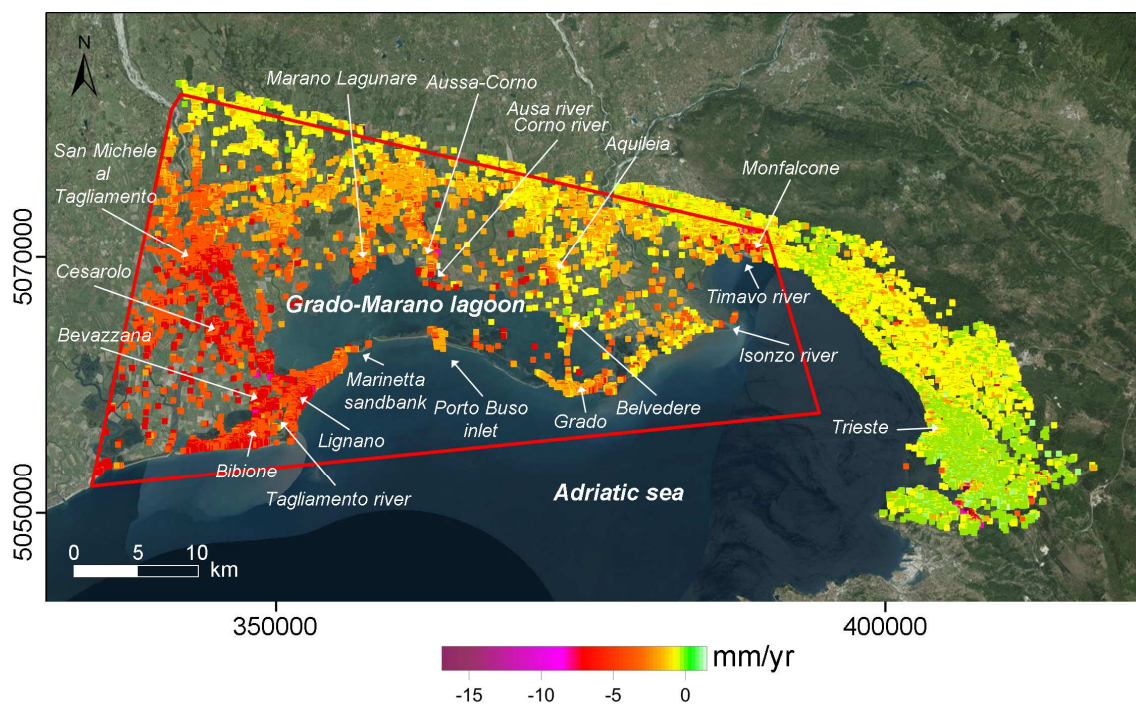
Station ID	Station Name	Longitude (deg)	Latitude (deg)	E (mm/yr)	N (mm/yr)	UP (mm/yr)	$CGPS_{LOS}$ (mm/yr)
PAZO	Palazzolo dello Stella (UD)	13° 03' 9.19"	45° 48' 20.60"	21.6	17.1	-1.3	-1.2
TRIE	Trieste	13° 45' 48.67"	45° 42' 35.12"	20.8	17.5	-0.5	-0.8
BEVA	Bevazzana (UD)	13° 04' 9.93"	45° 40' 18.81"	21.6	17.6	-4.4	-4.1

195

196

197 Finally, the differences between the  $CGPS_{LOS}$  and the velocities of the PTs (Point  
 198 Targets) averaged over a 200-m radius centered on the three CGPS stations were used  
 199 for the tilting plane (Tosi et al., 2015) implemented to correct the interferometric  
 200 products.

201 The velocity map of the ground movements of the FVG coast resulting from the  
 202 calibration and de-flattening of the Envisat ASAR PSI products available from the  
 203 Italian Ministry of the Environment and Protection of Land and Sea is shown in Fig. 2.  
 204 The analysis of coastal subsidence focuses on the coastal plain with ground elevations  
 205 of approximately less than 20 m above mean sea level (MSL), which includes nearly  
 206 22,000 PTs.  
 207



208  
 209 **Fig. 2.** Average land displacements obtained by PSI on Envisat ASAR images for the  
 210 2003-2010 period. Positive values indicate uplift, and negative values indicate land  
 211 subsidence. The area delimited by the red polygon is the coastal study area with ground  
 212 elevation lower than approximately 20 m above MSL.  
 213  
 214 The coastal plain is characterized by a gradient of subsidence increasing from the  
 215 northern margin of the study area toward the littoral along a rather well-defined

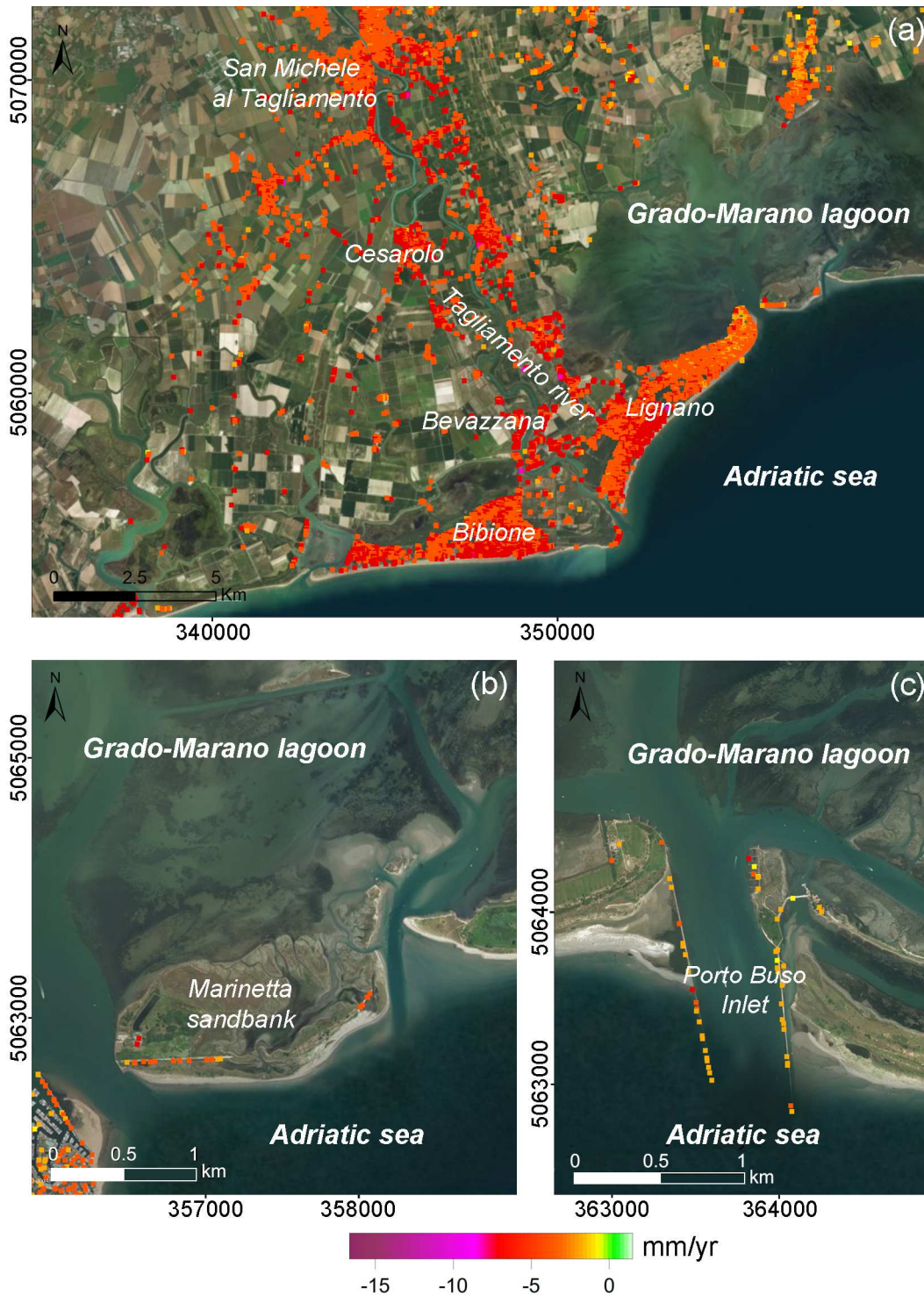
216 southwestern direction. Based on the relative stability of the upper portion, the average  
217 land subsidence rate increases to 2.5 mm/yr in the central part, at the boundary of the  
218 Grado-Marano lagoon, and to 4 mm/yr close to the Tagliamento River delta, where  
219 local settlements of up to 10 mm/yr have been detected.

220 A more detailed analysis of the land subsidence through a description of its behavior in  
221 the main sectors of the coastal plain is provided in the following.

222 Focusing on the littoral strip from Bibione to Monfalcone, the land subsidence trend  
223 clearly decreases eastward. However, high sinking values have been observed locally  
224 along the whole littoral. The littorals of Bibione and Lignano show quite homogeneous  
225 and significant subsidence, with average rates of approximately 4 mm/yr and local  
226 sinking of up to 10 mm/yr in the back sector of the delta at Cesarolo (Fig. 3a).  
227 Significant land subsidence rates affect the western narrow littoral separating the Grado-  
228 Marano lagoon from the Adriatic Sea, i.e., Isola Marinetta. Although statistically  
229 insignificant because only a few PTs are present, sinking values range from 2 to 4  
230 mm/yr (Fig. 3b). More PTs are present in the jetties of the Porto Buso inlet, and  
231 although a few of them sink by as much as 4 mm/yr, rather homogenous displacement  
232 rates with an average of -2 mm/yr characterize the inlet (Fig. 3c).

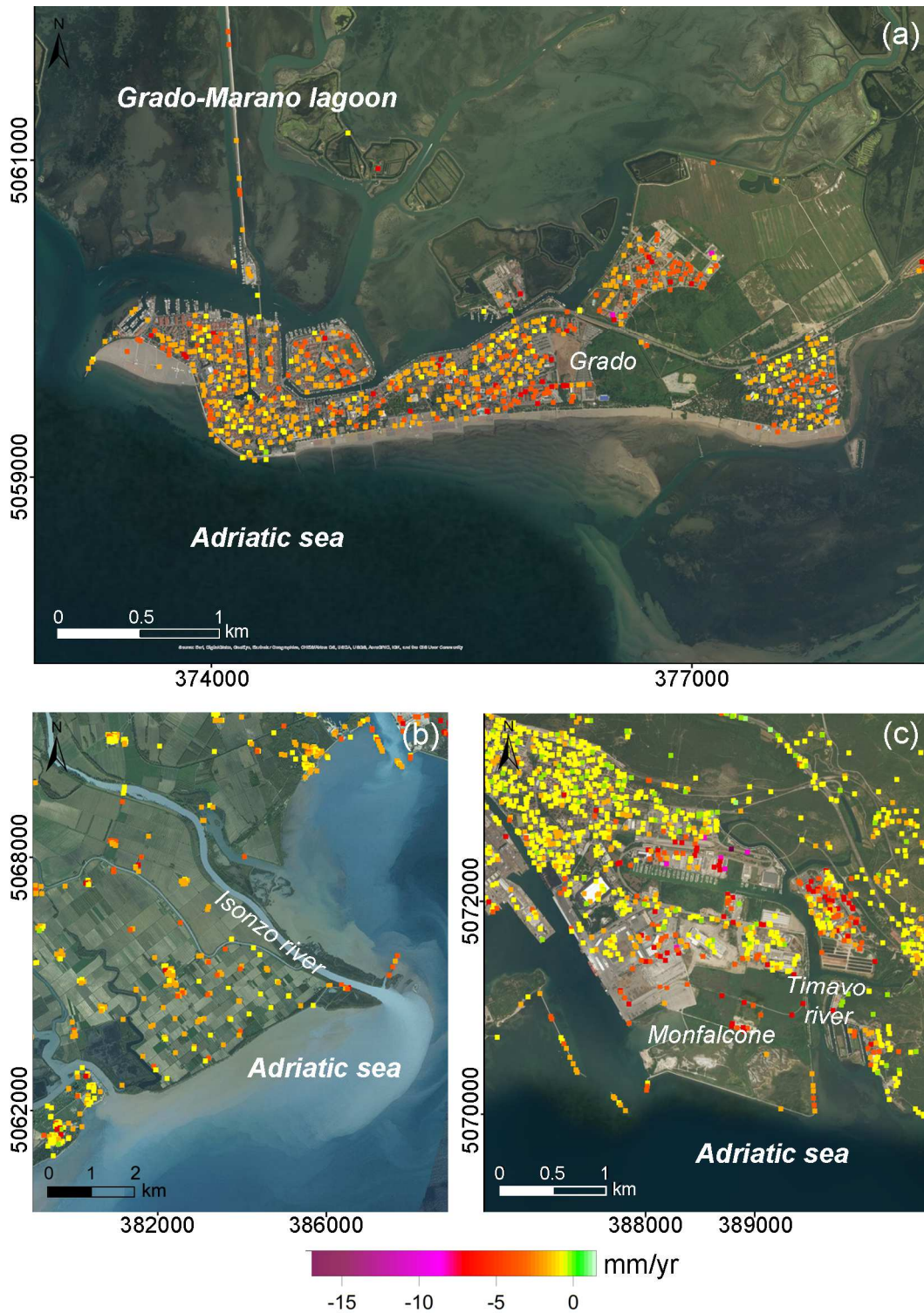
233 The subsidence of the eastern littoral sector encompassing Grado, the Isonzo River  
234 mouth and Monfalcone is punctuated by high variability. Although the average  
235 subsidence of such areas spans from 2 and 2.5 mm/yr (significantly lower than that of  
236 the Tagliamento River delta), sinking rates as high as 10 mm/yr at Grado (Fig. 4a), 4  
237 mm/yr in the Isonzo estuary (Fig. 4b) and 8 mm/yr in the Monfalcone industrial area  
238 (Fig. 4c) have been detected.

239



240

241 **Fig. 3.** Details of the average land displacements 2003-2010 at (a) Bibione and Lignano  
 242 littoral and San Michele al Tagliamento in the mainland; (b) Marinetta sandbank; and  
 243 (c) Porto Buso inlet. Positive values indicate uplift, and negative values indicate land  
 244 subsidence.



246

247 **Fig. 4.** Details of the average land displacements over the period 2003-2010 in the  
 248 littoral strip at (a) the Grado littoral; (b) the Isonzo River mouth; and (c) the Monfalcone

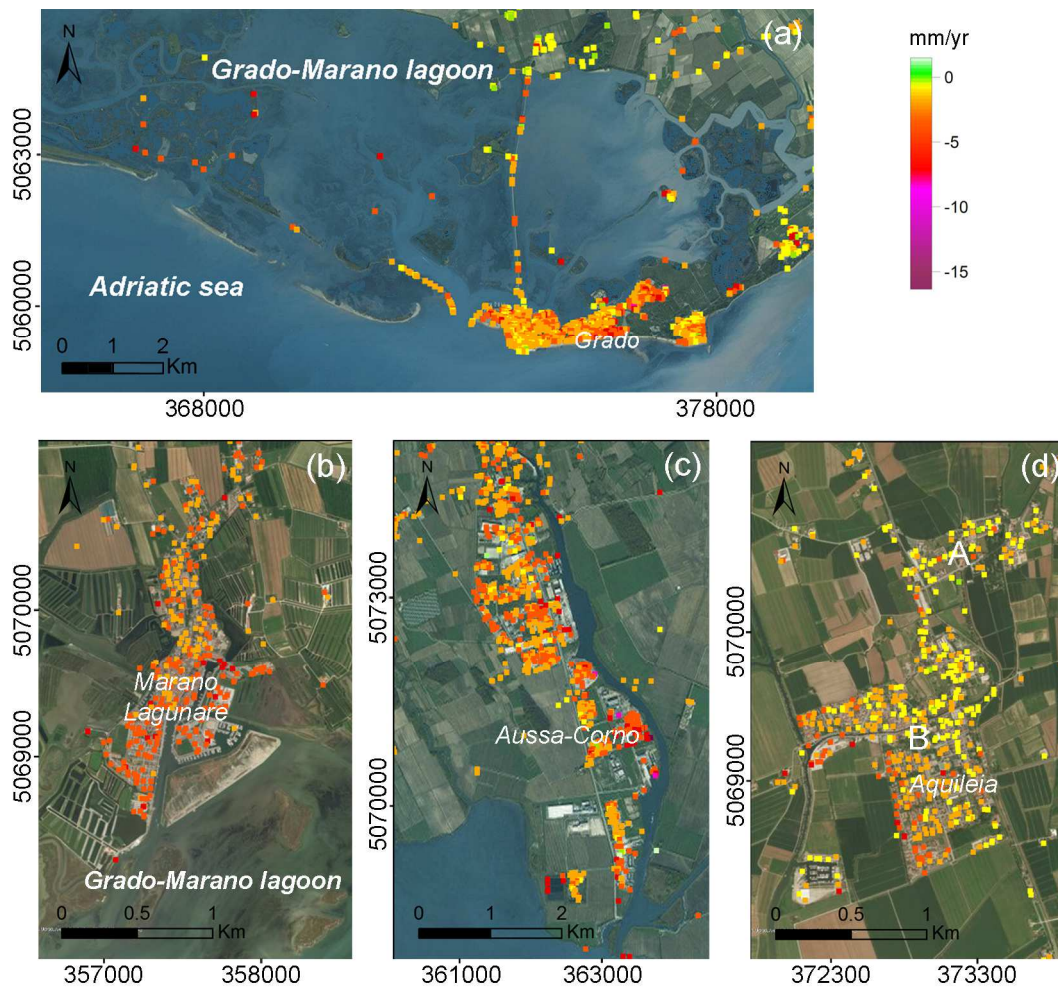
249 industrial port area. Positive values indicate uplift, and negative values indicate land  
250 subsidence.

251

252 Moving to the lagoon of Grado-Marano, the presence of PTs is very scarce and  
253 generally limited to a few scattered salt marshes, the embankments and the bridge. The

254 values of the displacements are quite variable, from a stable condition to approximately  
255 -5 mm/yr (Fig. 5a).

256



257

258 **Fig. 5.** Details of the average land displacements over the period 2003-2010 in the

259 lagoon of Grado-Marano and its northern margin: (a) the lagoon; (b) Marano Lagunare;

260 (c) the Aussa-Corno industrial area; and (d) Aquileia ancient city (A) and recent built-

261 up areas (B). Positive values indicate uplift, and negative values indicate land  
262 subsidence.

263

264 In the mainland bounding the northern margin of the lagoon between the Stella River  
265 mouth and the confluence of the Ausa and Corno River mouths, Marano Lagunare  
266 shows a peculiar subsidence pattern with the sinking rate increasing to 7 mm/yr toward  
267 the lagoon (Fig. 5b). In the eastern part of Marano Lagunare, uneven subsidence was  
268 detected in the industrial zone of Aussa-Corno (Fig. 5c). Although the average  
269 subsidence is approximately 2.5 mm/yr, the ground movements range from negligible  
270 values to more than -10 mm/yr.

271 Uneven sinking rates were also detected at Aquileia, which includes archeological and  
272 newly built-up areas. The newly developed residential district shows a sinking rate of  
273 approximately 4 m/yr, with some spots exhibiting rates as high as 5 mm/yr, while in the  
274 ancient city, established in Roman times, the land subsidence rate is generally lower  
275 than 2 mm/yr (Fig. 5d).

276 Moving to the mainland, the area most strongly affected by land subsidence is located  
277 between San Michele al Tagliamento and Bevazzana, where it averages approximately  
278 3.5 mm/yr, with homogeneous local sinking sectors exhibiting rates as high as 5 mm/yr  
279 (Fig. 3a).

280

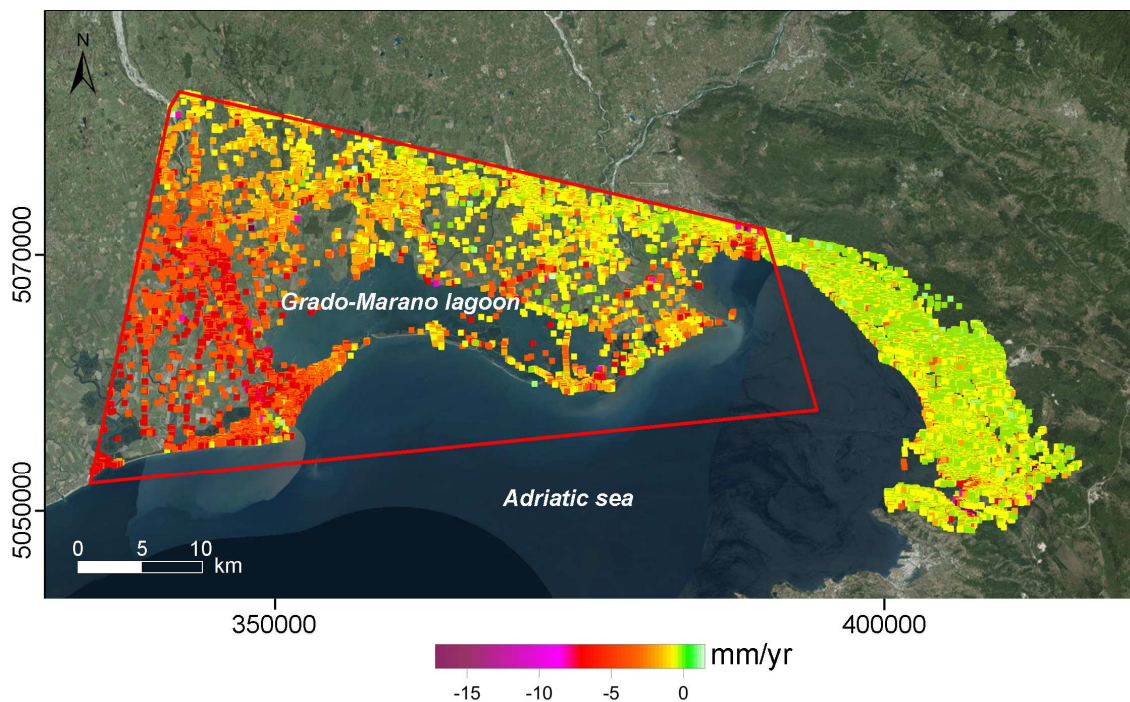
### 281 **3.2 Historical land subsidence over 1992-2000 period**

282 The availability of the SAR interferometric products retrieved by ERS1/2 images allows  
283 for the analysis of land subsidence to extend back to the 1992-2000 period (Fig. 6).

284 The ERS interferometric dataset was corrected and calibrated using a tilting plane  
285 model computed by the differences between SAR and ground-based velocities in three  
286 sites: Trieste, San Michele al Tagliamento and Belvedere. According to a number of  
287 studies based on long-term relative sea level data recorded at the tide gauge of Trieste  
288 (e.g., Carbognin et al., 2010; Carbognin et al., 2011), null ground movements were  
289 assumed at the tide gauge of Trieste for SAR data displacements. An average  
290 displacement of -4 mm/yr was assumed for the San Michele al Tagliamento site, as  
291 detected by the 1989-2002 leveling (e.g., Antonioli et al., 2009), and an average  
292 displacement of -1.2 mm/yr was assumed for the Belvedere site, whose subsidence rates  
293 remain nearly unchanged over the 1980-2004 period, as demonstrated by the 1980-1997  
294 and 1997-2004 levelling data (Marchesini, 2006). Because CGPS stations were absent  
295 during the ERS1/2 acquisition time span, correction due to differential horizontal  
296 displacements is not possible. However, considering that the study area is quite  
297 uniformly moving northeastward (Table 1) with respect to the plate motion and there is  
298 low sensitivity to the horizontal components of the displacement because the average  
299 incident angle of ERS1/2 acquisitions is approximately  $23^\circ$ , we can reasonably assume  
300 that the horizontal component of the LOS is negligible with respect to the vertical one.  
301



302



303

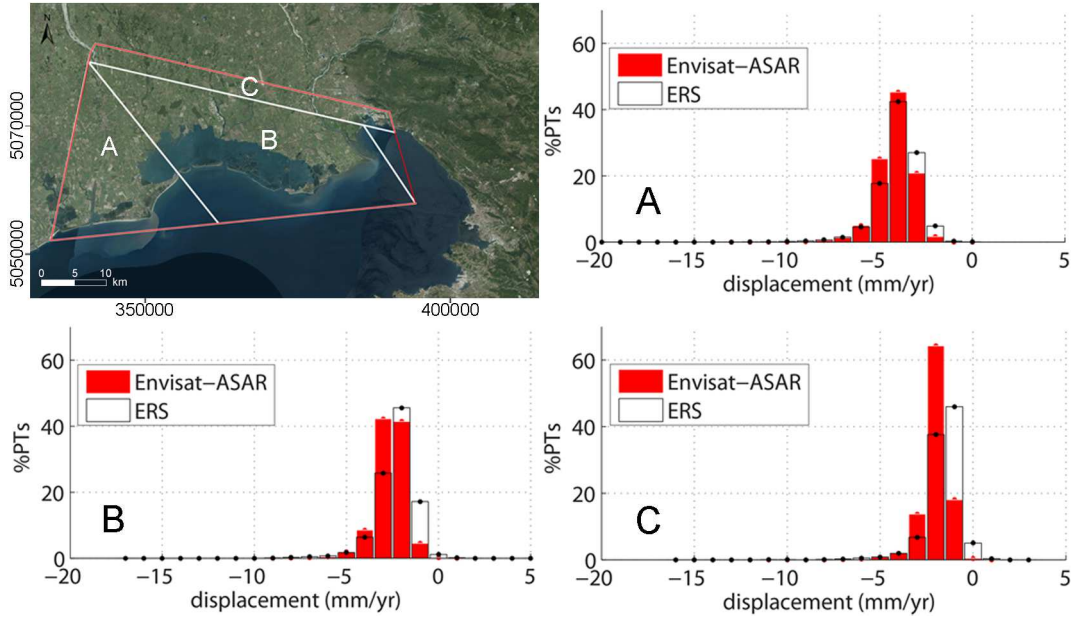
304 **Fig. 6.** Average land displacements obtained by PSI on ERS1/2 images for the 1992-  
305 2000 period. Positive values indicate uplift, and negative values indicate land  
306 subsidence. Red polygon bounds the coastal study area with ground elevation lower  
307 than approximately 20 m above MSL.

308

309 The image of the 1992-2000 ground displacements at the regional scale is quite similar  
310 to that obtained for the 2003-2010 period, i.e., an increasing subsidence trend toward  
311 the southwestern part of the FVG coastland. A more detailed analysis was performed  
312 comparing the ground velocities measured over the periods 1993-2000 and 2003-2010  
313 in three areas characterized by different land subsidence patterns, i.e., sectors A, B and  
314 C in Fig. 7. In the 2003-2010 period, the average land subsidence rates are  $3.7 \pm 0.9$   
315 mm/yr,  $2.1 \pm 0.9$  mm/yr and  $1.5 \pm 0.8$  mm/yr for areas A, B and C, respectively, while  
316 in the previous time span the average land subsidence rates are  $3.5 \pm 1.2$  mm/yr,  $1.8 \pm$

317 1.1 mm/yr, and  $1.1 \pm 1.0$  mm/yr, respectively. The frequency distributions of these  
 318 average displacement rates are shown in Fig. 7.

319



320

321 **Fig. 7.** Frequency distribution of the 1993-2000 (white) and 2003-2010 (red) average  
 322 ground movement rates in sectors A, B, and C of the FVG coastal plain shown in the  
 323 satellite image.

324

325 To quantify the land movement differences at the regional scale between the 2003-2010  
 326 and 1992-2000 time spans, two calibrated and de-flattened interferometric solutions  
 327 were interpolated using the Kriging method on the same regular 500-m grid, i.e., a  
 328 compromise based on the distribution of the displacement data, covering the considered  
 329 coastal plain. Then, the land subsidence change ( $\delta$ ) was computed for each node (Eq.  
 330 2):

331

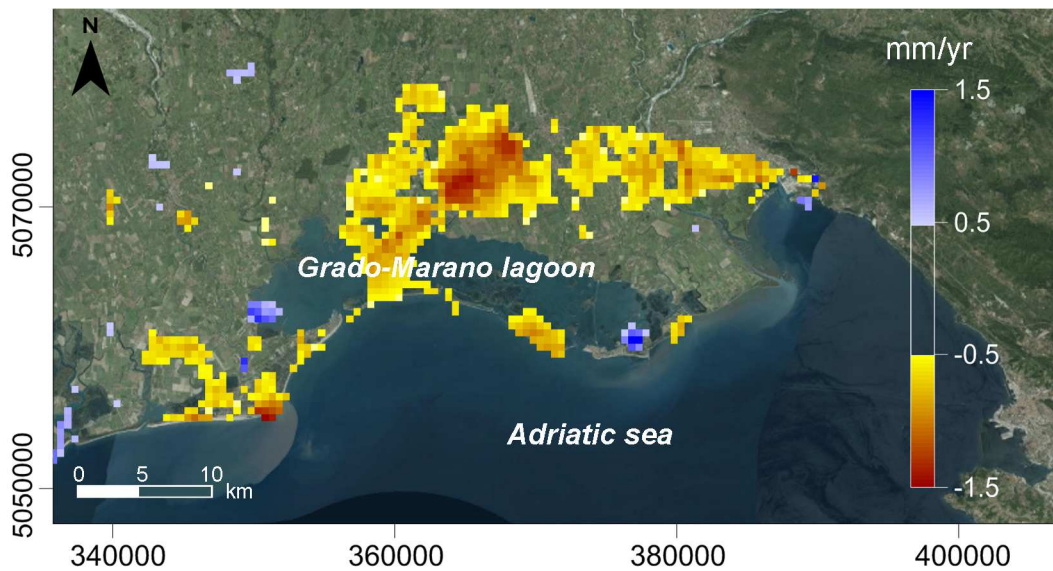
$$\delta = \lambda_{2003-2010} - \lambda_{1992-2000} \quad (2)$$

332

where  $\lambda_{2003-2010}$  and  $\lambda_{1992-2000}$  are the interpolated land velocity values.

333 It should be noted that for a more correct quantification of the two subsidence datasets,  
334 the relatively large area of Grado-Marano lagoon not covered by PTs was removed for  
335 this type of analysis.

336



337

338 **Fig. 8.** Land subsidence change ( $\delta$ ) obtained by the difference between the 2003-2010  
339 and 1992-2000 velocities interpolated on a regular 500-m grid.

340

341 The results show  $\delta$  values ranging from 0.8 to -1.3 mm/yr (Fig. 8). These findings  
342 indicate that, despite slight increases in land subsidence in the central part of the study  
343 area, any other consideration of the velocity changes is almost speculative, as the values  
344 are within the range of uncertainty, i.e., the incorporation of the SAR method affects the  
345 assumptions made in the calibration procedures and the interpolation models.

346

### 347 **3.3 Long-term land subsidence over the 1992-2010 period**

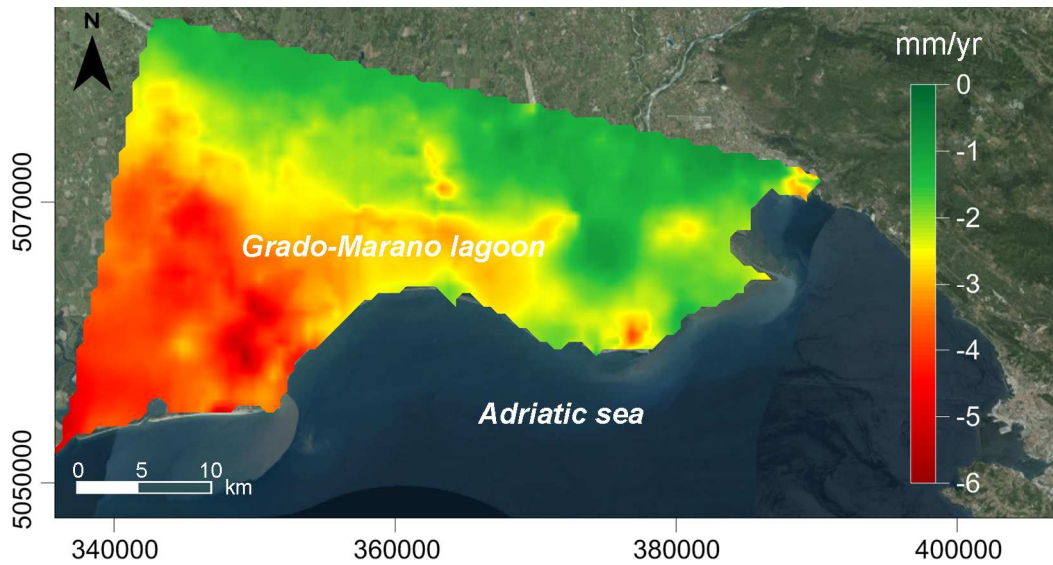
348 The average land velocity map for the period 1992-2010 (Fig. 9) was obtained as  
349 follows. First, cumulative land subsidence from 1992 to 2010 ( $\Lambda_{1992-2010}$ ) was computed  
350 for each grid node as follows (Eq. 3):

$$351 \quad \Lambda_{1992-2010} = 11 \cdot \lambda_{1992-2000} + 8 \cdot \lambda_{2003-2010} \quad (3)$$

352 where 11 and 8 are the time spans considered to compute the displacements. It should  
353 be noted that the cumulative land subsidence from 1992 to 2000 obtained by ERS1/2  
354 was multiplied by 11 years, assuming the same average velocities for the period 2001-  
355 2002. The long-term land subsidence between 1992 and 2010 ( $\bar{\Lambda}_{1992-2010}$ ) was then  
356 derived as the mean value over the total time frame of 19 years; the modeling outcome  
357 is shown in Fig. 9.

358 The  $\bar{\Lambda}_{1992-2010}$  map confirms the general increasing trend toward the southwestern part  
359 of the study area close to the Tagliamento River and the significant heterogeneity of the  
360 subsidence in the coastal plain at the regional scale, with velocities spanning from less  
361 than 1 mm/yr to more than 5 mm/yr. Notably, the interpolated map provides a reliable  
362 image of the land subsidence at the regional scale as it significantly smooths local high  
363 sinking also present where average values are not particularly high.

364



365

366 **Fig. 9.** Long-term land subsidence  $\bar{\Lambda}_{1992-2010}$  computed on a regular 500-m grid for the  
 367 1992-2010 period. Positive values indicate uplift, and negative values indicate land  
 368 subsidence.

369

#### 370 **4. Discussion**

##### 371 **4.1 Regional subsidence**

372 This study depicts an image of the land subsidence of the FVG coastal plain delineating  
 373 a regional gradient that increases seaward, with maximum sinking rates in the area  
 374 adjacent to the Tagliamento River delta and various local heterogeneities superposed.

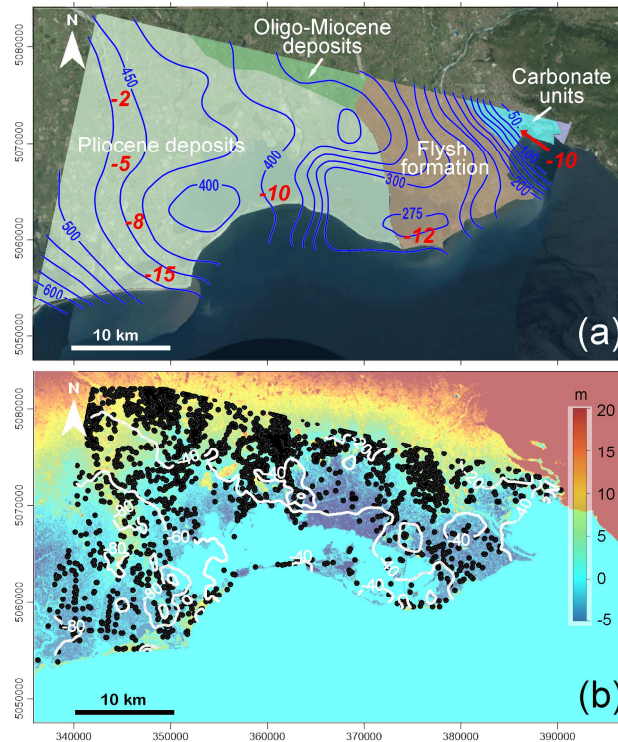
375 Land subsidence is the result of natural processes and anthropogenic activities, hardly  
 376 quantifiable separately but whose prevailing contributions are likely identifiable.  
 377 Tectonics (including Glacial Isostatic Adjustment-GIA and bedrock accommodation)  
 378 and compaction of the subsoil are among the main natural components of regional land  
 379 subsidence.

380 In the FVG region, the high-subsidence sectors (Fig. 2, Fig. 6, Fig. 9) are well  
 381 correlated with the deeper base of the Pre-Quaternary deposits (Fig. 10a). Moreover,

382 considering the FVG plain divided by the Dinaric thrust in two main sectors  
383 corresponding to the different bedrock types, i.e., the Pliocene and Flysh formation (Fig.  
384 10a) (Busetti et al., 2009), the higher sinking zone is located in the former.

385 Regarding the component of the land subsidence due to the shallow subsoil  
386 geomechanical characteristics, recent studies have noted that in many coastal plains the  
387 compaction of the younger Holocene subsoil is significantly higher than that of the  
388 Pleistocene sediments (Törnqvist et al., 2008; Higgins et al., 2014). This correlation has  
389 also been observed for the Holocene marine-lagoon and the alluvial last glacial  
390 maximum (LGM) and pre-LGM deeper deposits by Tosi et al. (2009) and Teatini et al.  
391 (2011) in the Venice and Po delta regions, respectively. However, the high-sinking  
392 sectors and the major thickness of the Holocene deposits are not correlated everywhere  
393 in the FVG coastal plain (Fig. 10a,b) as in the higher course of the Tagliamento River  
394 (San Michele al Tagliamento area), where the major contribution to the subsidence is  
395 due to groundwater exploitation.

396



397

398 **Fig. 10.** Geologic and morphologic setting of the study area. (a) Map of the depth (m) of  
 399 the Quaternary base (blue contour lines) (from Regione Friuli Venezia Giulia, 2014)  
 400 superimposed on the units of Pre-Quaternary deposits (from Busetti et al., 2009). Red  
 401 numbers refer to the approximate thickness (m) of Holocene deposits (from Amorosi et  
 402 al., 2008; Bondesan et al., 2008; Marocco and Melis, 2009; Trobec et al., 2017). (b)  
 403 Map of cumulative land subsidence  $\Delta_{1992-2010}$  (mm) (white contour lines) over the 1992-  
 404 2010 period superimposed on the elevation map of the coastland (SRTM 1 Arc-Second  
 405 data from USGS Earth Resources Observation and Science (EROS) Center). Black dots  
 406 refer to the groundwater well positions (from Regione Friuli Venezia Giulia, 2014).

407

408 Regarding the induced subsidence, groundwater withdrawals, hydraulic reclamations  
 409 and urbanization are the most common causes of land subsidence. In the FVG coastal  
 410 plain, groundwater is exploited for various purposes (e.g., drinking, agricultural,  
 411 industrial, fish breeding) from a multilayer aquifer system consisting of six main

412 aquifers down to a depth of approximately 500 m (Rapti-Caputo et al., 2009; Zini et al.,  
413 2013). In the deeper aquifers, particularly those close to Tagliamento River delta,  
414 thermal waters are also exploited (Stefanini et al., 1976; Stefanini et al., 1977; Stefanini  
415 et al., 1978). The western areas are the most significantly subsiding sectors (Fig. 2). In  
416 particular, the areas adjacent to the Tagliamento River course, such as San Michele al  
417 Tagliamento, Cesarolo and Bevazzana, show sinking rates as high as 5 mm/yr and  
418 locally greater values. Groundwater is exploited in the NW sector as well, but the  
419 presence of a low-compressibility gravel-sand rich subsoil likely renders land  
420 subsidence negligible (averages to 0.7 mm/yr) (Fig. 2). Similar subsidence rates  
421 characterize the Venice high plain, close to the alpine foothills, which shows analogous  
422 characteristics with respect to the subsoil setting and groundwater use (Tosi et al.,  
423 2016).

424 A study including, for instance, measurements of groundwater levels, groundwater  
425 pumping and aquifer recharge should be conducted to quantify the role of groundwater  
426 exploitation in driving land subsidence, based on the groundwater use provided by Treu  
427 (2011). However, we highlight that in higher sinking areas such as the Tagliamento  
428 River course, the littoral of Grado and the northern lagoon margin, a significant number  
429 of wells are present. Nevertheless, it should be noted that a high density of wells is also  
430 located in the northern plain, where land subsidence is negligible. This issue also  
431 concerns the Venice area (Da Lio et al., 2013; Da Lio et al., 2015) and the Po River  
432 delta, where updating of the groundwater monitoring network and quantification of  
433 pumping are necessary to understand unclear local and regional subsidence patterns  
434 (Tosi et al., 2016).



435 High subsidence rates are also typically common in low-lying coastlands corresponding  
436 to ancient marshes and lagoons, today hydraulically drained and transformed into  
437 farmlands. Land subsidence in such environments generally combines the compaction  
438 of the relatively recent soft deposits with the loss in ground elevation due to oxidation  
439 of peaty soils driven by hydraulic reclamation and agricultural activities (Gambolati et  
440 al., 2005; Deverel et al., 2016; Zhou et al., 2016). In the FVG coastal plain, a clear  
441 correlation between the low-lying reclaimed areas and the higher land subsidence  
442 sectors is found only in the western lowlands corresponding to the lower Tagliamento  
443 River course but not in the central and eastern sectors, where subsidence is not  
444 significant (Fig. 10). One possible explanation of this low sinking is the presence of  
445 exposed LGM and pre-LGM deposits (Fontana et al., 2008; Fontana et al., 2010;  
446 Zanferrari et al., 2014) rather than the younger Holocene back-barrier deposits.  
447 Moreover, the analysis of these low-lying sectors may have been biased because of the  
448 presence of PTs mainly in stable structures, i.e., located on sandy layers (e.g., paleo-  
449 channels) not involved in the organic soil oxidation or founded in deep subsoil, rather  
450 than in the farmlands where the C-band sensors are typically unusable for measuring  
451 land movements because of the presence of vegetation. This issue has already been  
452 noted by Teatini et al. (2005) and Teatini et al. (2007) in similar vegetated areas of the  
453 Veneto coastal plain and partly overcome by combining L-band and X-band sensors  
454 (Tosi et al., 2016) and using artificial corner reflectors (Strozzi et al., 2013).

455

#### 456 **4.2 Comparison with adjacent similar hydro-geomorphologic settings**

457 Land subsidence of the FVG coastal plain has been compared with that of the adjacent  
458 Venice - Po River delta region under similar hydro-geomorphologic settings of the  
459 littoral and mainland sectors.

#### 460 *4.2.1 Littoral sector*

461 The Tagliamento delta (Fig. 3a) is characterized by an average subsidence rate of  
462 approximately 4 mm/yr, which is significantly lower than the rates of up to 10-15  
463 mm/yr measured in the Po River delta lobe by Teatini et al. (2011) and Tosi et al.  
464 (2016). The higher thickness of the Holocene highly compressible prodelta muds and  
465 the very fast delta progradation occurring over the past 500 years (Sestini, 1996; Teatini  
466 et al., 2011; Tosi et al., 2016) make the Po River deltaic area more prone to sinking than  
467 the Tagliamento River deltaic area, although groundwater exploitation should contribute  
468 to the sinking area around Bibione and Lignano (Tosi et al., 2007). In contrast, land  
469 subsidence at the Piave and Tagliamento River mouths (Tosi et al., 2016) is more  
470 comparable because of the similar subsoil and land use characteristics of the regions.

471 Moving to the eastern littoral strip bounding the Grado-Marano lagoon (Fig. 3b,c), the  
472 average land subsidence of the Marinetta sandbank is approximately 2.5 mm/yr. Most  
473 of the PTs refer to the stone embankments built for protecting the littoral from erosion  
474 and storm waves. This value is quite similar to that measured in the older stone  
475 embankments bounding the fish farms at the Cavallino – Treporti littoral (Venice),  
476 where sandy layers prevail in the shallow subsoil (Tosi et al., 2010). The jetties built in  
477 the early 1960s at Porto Buso inlet show slow sinking rates of approximately 2 mm/yr,  
478 similar to those occurring in the older and well-consolidated parts of the jetties of the  
479 Venice lagoon inlets, which were not addressed by recent MoSE studies (Strozzi et al.,  
480 2009; Tosi et al., 2012).

481 The littoral of Grado (Fig. 4a), a sector mostly devoted to tourism, shows uneven  
482 subsidence due to the combination of subsoil heterogeneity, groundwater exploitation  
483 and loads induced by newly built-up sectors, quite similar to the characteristics detected  
484 at Jesolo (northern Venice littoral), where analogous subsidence driving mechanisms  
485 are present (Tosi et al., 2015).

486 The variability of the land subsidence measured at the Isonzo River mouth, ranging  
487 from 0.5 to 5 mm/yr (Fig. 4b), reflects the heterogeneity of the shallow subsoil related  
488 to i) the coastal evolution of the littoral - back barrier system over the early Holocene  
489 and ii) the later eastward shifting of the river mouth to the current position. These  
490 features have provided opportunities to reclaim wetlands, often rich in organic deposits,  
491 today (Marocco, 1989).

492 High variability of land subsidence (from less than 1 to 6-8 mm/yr) also characterizes  
493 the easternmost part of the coastal sector corresponding to the Monfalcone industrial  
494 and harbor area (Fig. 4c). Groundwater extraction for industrial and geothermal use  
495 (Treu, 2011) along with the load of infrastructures and facilities are likely the causes of  
496 the major distribution of land sinking, while the subsoil architecture plays an important  
497 role in shaping subsidence heterogeneity. The marshy area located at the foot of the  
498 Karst near the mouth of the Timavo River (Monfalcone) corresponds to a Roman time  
499 large lagoon (e.g., *Insulae Clarae*, *Lacus Timavi*) progressively filled by sandy-pelite  
500 marine and alluvial deposits (e.g., Marocco and Melis, 2009) to form a salt marsh  
501 environment, recently reclaimed to develop the industrial area. The carbonate bedrock  
502 lies at depths of 30-40 m and 10-20 m in the eastern and western sector, respectively  
503 (e.g., Marocco and Melis, 2009). As the land subsidence rates for the active residual  
504 consolidation increase, the infilling thickness of the ancient lagoon basin increases.

#### 505 4.2.2 Lagoon sector

506 Most of the PTs refer to land subsidence because even a small loss in ground elevation  
507 combined with the increasing sea level rise may threaten its survival. The intrinsic  
508 capacity of salt marshes to keep pace with the relative sea level rise (Rizzetto and Tosi  
509 2011; Rizzetto and Tosi 2012) largely depends on soil compaction and sediment  
510 availability (Zoccarato et al., 2017) as well as bio-morphological processes (Marani et  
511 al., 2013). The subsidence of the Grado-Marano lagoon averages approximately 2  
512 mm/yr (Fig. 5), although salt marshes and lagoon embankments sink more rapidly  
513 because of multiple causes, which include natural consolidation of different thicknesses  
514 of Holocene subsoil, groundwater exploitation and likely the instability of embankments  
515 bounding the northern lagoon margin (Fontolan et al., 2012). Similar behavior  
516 characterizes the lagoons of Venice and the Po River delta (Tosi et al., 2010; Tosi et al.,  
517 2016; Da Lio et al., 2018). The scarcity of PTs in the Grado-Marano lagoon related to  
518 the temporal decorrelation of the radar signal due to the presence of vegetation do not  
519 allow for a detailed analysis or quantification. Further application of ad hoc SAR  
520 strategies, i.e., the use of artificial corner reflectors and the combination of the X and L  
521 bands, as various authors have recently tested (Nitti et al., 2009; Strozzi et al., 2013;  
522 Luo et al., 2014; Tosi et al., 2016; Da Lio et al., 2018), could be crucial to overcome  
523 this limitation.

#### 524 4.2.3 Mainland sector

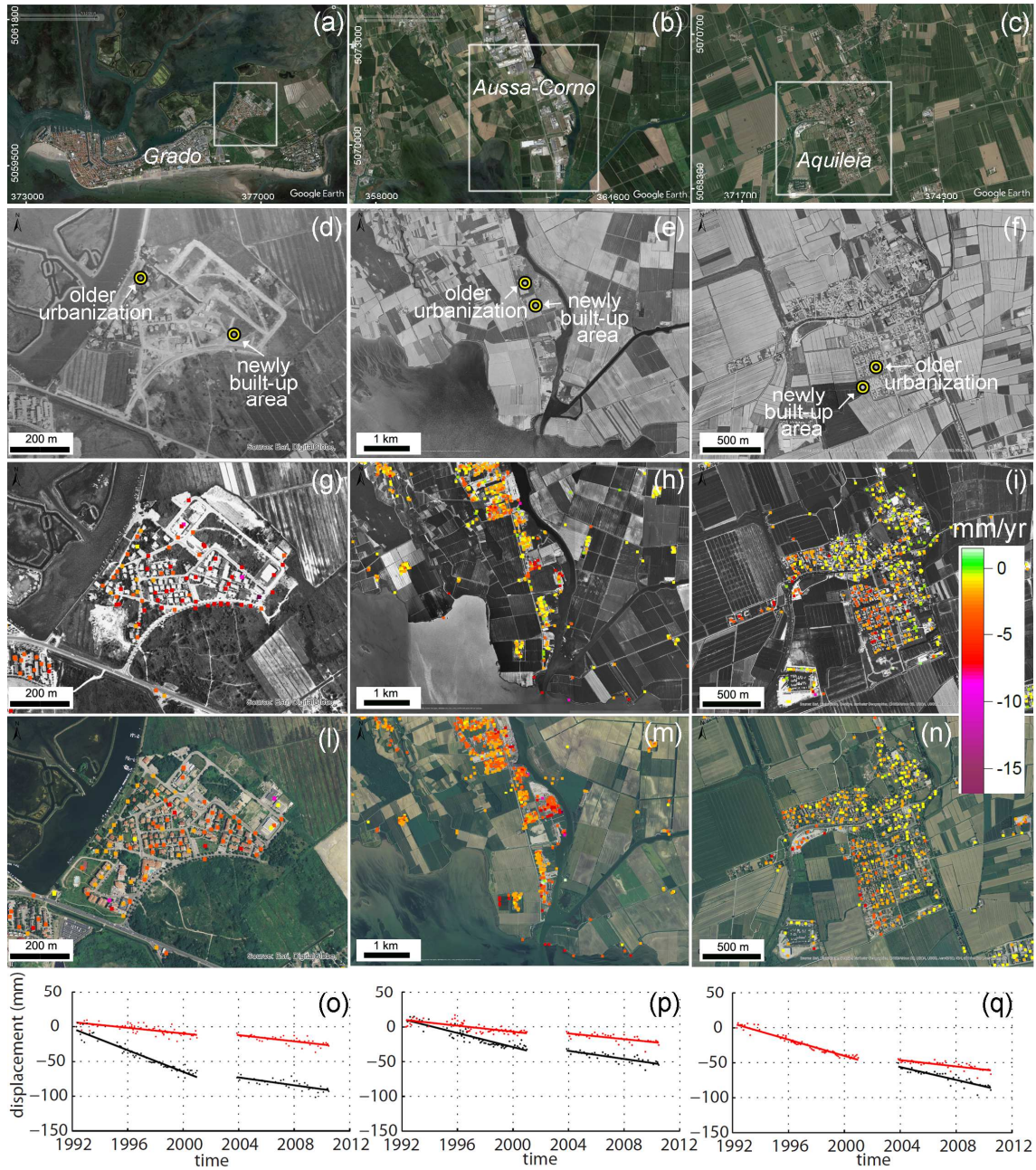
525 The subsidence of the mainland bounding the northern lagoon margin ranges from a  
526 stable condition to 8 mm/yr (Fig. 2). In the western margin (e.g., Bevazzana, Cesarolo,  
527 San Michele al Tagliamento in Fig. 3a), groundwater is widespread, and spatially  
528 marked variations in subsidence do not occur, while in the central and eastern margins,

529 the new built-up areas (e.g., Marano Lagunare, Aussa-Corno, Aquileia in Fig. 5b,c,d)  
530 show extensive sinking. The transition from marine-lagoon Holocene deposits to the  
531 alluvial units is strongly correlated with the heterogeneity of ground movements. The  
532 archaeological area of Aquileia, which is on the UNESCO World Heritage Sites List for  
533 Early Roman Empire and Middle Age remnants, requires particular attention. Ground  
534 movements are quite negligible, whereas sinking sectors reaching subsidence rates as  
535 high as 5 mm/yr are detected in the newly urbanized areas (Fig. 5d). This finding  
536 reflects the diverse consolidation history and the dominantly clayey subsoil in the newly  
537 built-up area (Alfarè et al., 2014). Similar subsidence behavior has been detected in the  
538 archaeological area of Altino (Carbognin et al., 1995; Tosi et al., 2016), located in the  
539 NW Venice lagoon margin and in the historical center of Venice and Chioggia (Tosi et  
540 al., 2016), where the consolidation rate of ancient well consolidated deposits is 0.5-1  
541 mm/yr and only the newly built-up sites locally show high sinking rates. A different  
542 situation characterizes the coastal area of Ravenna (Emilia-Romagna region), where  
543 groundwater exploitation has induced severe land subsidence: More than 1 m  
544 accumulated during the 1950-1980 period at Porta Adriana in the historical center of  
545 Ravenna, and rates as high as 40 mm/yr were measured in 1972-1977 in the area of  
546 Lido di Classe (Teatini et al., 2005 and reference therein), where the former port  
547 established in the Roman period was located (Mauskopf Deliyannis, 2010).

548 As urbanization is often a cause of land subsidence in coastal plains, as the new loads  
549 associated with buildings on relatively recent deposits induce their consolidation even  
550 over periods longer than one decade (Yan et al., 2002; Bianchini et al., 2015; Chen et  
551 al., 2015; Erkens et al., 2015), we report three cases of sinking sectors due to newly  
552 built-up areas, i.e., the eastern part of the Grado littoral facing the lagoon, the Aussa-

553 Corno industrial area and Aquileia along the northern lagoon margin (Fig. 11). The  
554 correlation between the high subsidence rates and the age of the construction of the  
555 buildings is clearly demonstrated by the average land displacements maps. Over the  
556 1992-2000 period, the newly built-up areas established during the end of the 1980s and  
557 the beginning of 1990s experienced higher subsidence rates than did the nearby sectors  
558 where urbanization is older (Fig. 11). Reduced sinking appears to characterize the later  
559 period. Similar behavior has been observed in the Venice area by Tosi et al. (2015) at  
560 Chioggia and Jesolo, where local bowls showing subsidence rates of up to 10 mm/yr—  
561 associated with the construction of new large buildings—have been detected.

562



563

564 **Fig. 11.** Land displacements in older and newly built-up areas at (a) the Grado littoral;  
 565 (b) Aussa-Corno; and (c) Aquileia. The 1989 (d-f), 1994 (g-i) and 2006 (l-n) aerial  
 566 photograph bases are used as references for older urbanization and the 1992-2000 and  
 567 2003-2010 ground displacement velocities, respectively. Positive values indicate uplift,  
 568 and negative values indicate land subsidence. Examples of land displacement time

569 series (1992-2010) in older urbanization (red) and newly built-up areas (black) at (o) the  
570 Grado littoral; (p) Aussa-Corno; and (q) Aquileia.

571

## 572 **5. Conclusions**

573 The FVG coastal plain, similarly to most low-lying coastal plains worldwide, is highly  
574 sensitive to the loss in elevation due to sea level rise and land subsidence. While the  
575 subsidence of the main Adriatic coastal plains has been monitored for more than a  
576 century, in the FVG coastland, the process is still poorly understood. This study  
577 characterized land subsidence of this coastal region, improving knowledge of the  
578 ground vertical displacement dynamics.

579 Detailed land subsidence maps of the entire FVG coastal plain, with high spatial  
580 resolution and good accuracy, have been obtained by SAR-based interferometric  
581 datasets covering the 1992-2010 period as a result of their calibrations and corrections.  
582 Although this study does not aim to rigorously quantify the various components acting  
583 on the process, likely potential land subsidence driving mechanisms have been proposed  
584 and discussed, considering the various morpho-hydro-geological settings of the FVG  
585 coastal plain.

586 The main outcomes are summarized as follows:

- 587 • Calibrated SAR-based interferometry provided an original and comprehensive  
588 mapping of land subsidence in the FVG coastland during the study period,  
589 allowing for both “regional-” and “local-” (few km<sup>2</sup>) scale high-resolution data  
590 in areas never investigated previously because of the lack of leveling lines.
- 591 • On average, land subsidence rates range from less than 1 mm/yr to 5 mm/yr,  
592 with some PTs exhibiting rates greater than 10 mm/yr.



- 593       • The cumulative land subsidence over the period 1992-2010 reaches 100 mm.
- 594       • The comparison between land subsidence occurring during the period 2003-2010
- 595       and that occurring during the period 1992-2000 reveals no significant changes.
- 596       • A regional subsidence gradient increasing SW from the inland toward the coast
- 597       is correlated with the different geological settings forming the various sectors of
- 598       the coastal plain.
- 599       • The regional land subsidence mainly depends on geologic characteristics, such
- 600       as the bedrock setting and the thickness of the Holocene deposits.
- 601       • Land subsidence heterogeneities occurring at the local scale are likely related to
- 602       land use, including groundwater exploitation, and these local effects are
- 603       superposed onto the regional trend mainly driven by the subsoil setting.
- 604       • The newly built-up areas show higher subsidence rates than other areas, which
- 605       generally decrease over time. Nevertheless, after two decades, these areas are
- 606       subsiding more strongly than are the nearby sectors, where urbanization is more
- 607       established.
- 608       This study clearly highlights the need to update the analysis of land subsidence in the
- 609       FVG coastland for improving data coverage as well as distinguishing and quantifying
- 610       natural and anthropogenic driving processes. This issue should be addressed by the new
- 611       generation of satellite SAR platforms combined with an analysis of interferometric
- 612       products from different bandwidth sensors. In addition, the installation of a proper
- 613       network of artificial corner reflectors will allow for the detection of ground movements
- 614       in the inner lagoon, where radar reflecting structures are lacking.
- 615       In conclusion, the new knowledge on land subsidence in the FVG region encourages
- 616       further monitoring investigations aimed at improving the numerical simulation of land

617 subsidence and alternative management scenarios for sustainable groundwater  
618 exploitation. Specifically, these investigations should include monitoring of  
619 groundwater levels, quantification of groundwater pumping and aquifer recharge  
620 together with an accurate analysis of the land use changes occurring over the past  
621 decades. Although subsidence is not particularly severe in the FVG coastland, further  
622 loss of elevation with respect to the mean sea level will likely exacerbate the effect of  
623 other processes such as coastline erosion, coastal inundation and saltwater intrusion,  
624 with serious social and environmental impacts that are also related to expected global  
625 climate change.

626

#### 627 **Acknowledgements**

628 This work has been developed in the framework of the Flagship Project RITMARE -  
629 The Italian Research for the Sea - coordinated by the Italian National Research Council  
630 and funded by the Italian Ministry of Education, University and Research within the  
631 National Research Program 2011–2013. Data courtesy: Italian Ministry of the  
632 Environment and Protection of Land and Sea, within the framework of the Special Plan  
633 of Remote Sensing of the Environment for Envisat interferometric data (CC BY-SA 3.0  
634 IT); GPS time series, Nevada Geodetic Laboratory (NGL), available at  
635 <http://geodesy.unr.edu/>; terrain model SRTM 1 Arc-Second from NASA JPL., 2013,  
636 NASA Shuttle Radar Topography Mission Global 1 arc second Version 3. NASA  
637 EOSDIS Land Processes DAAC, USGS Earth Resources Observation and Science  
638 (EROS) Center, Sioux Falls, South Dakota (<https://lpdaac.usgs.gov>), accessed October  
639 27, 2017, at <https://doi.org/10.5067/measures/srtm/srtmg11.003>.

640

641 **References**

- 642 Abidin, H., Andreas, H., Gumilar, I., Fukuda, Y., Pohan, Y. E., Deguchi, T., 2011. Land  
643 subsidence of Jakarta (Indonesia) and its relation with urban development. *Nat.*  
644 *Hazards*. 59:1753-1771. <https://doi.org/doi:10.1007/s11069-011-9866-9>.
- 645 Alfarè, L., Donnici, S., Marini, M., Moscatelli, M., Tosi, L. Vallone, R., 2014. The  
646 Impact of Land Subsidence on Preservation of Cultural Heritage Sites: The Case  
647 Study of Aquileia (Venetian-Friulian Coastland, North-Eastern Italy). In: G.  
648 Lollino, A. Manconi, J. Locat, Y. Huang, M. Canals Artigas (Eds), *Engineering*  
649 *Geology for Society and Territory* (pp. 179-182). Vol 4. Springer, Cham.  
650 [https://doi.org/doi:10.1007/978-3-319-08660-6\\_34](https://doi.org/doi:10.1007/978-3-319-08660-6_34).
- 651 Amorosi, A., Fontana, A., Antonioli, F., Primon, S., Bondesan, A., 2008. Post-LGM  
652 sedimentation and Holocene shoreline evolution in the NW Adriatic coastal area.  
653 *GeoActa*. 7:41-67.
- 654 Antonioli, F., Ferranti, L., Fontana, A., Amorosi, A. M., Bondesan, A., Braitenberg, C.,  
655 Dutton, A., Fontolan, G., Furlani, S., Lambeck, K., Mastronuzzi, G., Monaco, C.,  
656 Spada, G., Stocchi, P., 2009. Holocene relative sea-level changes and vertical  
657 movements along the Italian and Istria coastlines. *Quatern. Int.* 206:102-133.  
658 <https://doi.org/doi:10.1016/j.quaint.2008.11.008>.
- 659 Bianchini S., Moretti S., 2015. Analysis of recent ground subsidence in the Sibari plain  
660 (Italy) by means of satellite SAR interferometry-based methods. *International J.*  
661 *Remote Sens.* 36:4550-4569. <https://doi.org/doi:10.1080/01431161.2015.1084433>.
- 662 Bondesan, A., Primon, S., Bassan, V., Vitturi A., 2008. *Le unità geologiche della*  
663 *provincia di Venezia* (177pp). Verona: Cierre Edizioni.

664 Busetti, M., Volpi, V., Nicolich, R., Barison, E., Romeo, R., Baradello, L., Brancatelli,  
665 G., Giustiniani, M., Marchi, M., Zanolla, C., Wardell, N., Nieto, D., Ramella, R.,  
666 2010. Dinaric tectonic features in the Gulf of Trieste (northern Adriatic Sea).  
667 *Bollettino di Geofisica Teorica ed Applicata*. 51:117-128.

668 Carbognin L., Tosi L., Teatini P., 1995. Analysis of actual land subsidence in Venice  
669 and its hinterland (Italy). In: F. B. J. Barends, F. J. J. Brouwer, F. H. Schröder,  
670 Land Subsidence: Natural causes, measuring techniques, The Groningen Gasfields  
671 (pp. 129-137). A.A. Balkema-Brookfield, Rotterdam, Netherlands.

672 Carbognin, L., Tosi, L., 2002. Interaction between climate changes, eustacy and land  
673 subsidence in the North Adriatic Region, Italy. *Mar. Ecol.* 23:38-50.  
674 <https://doi.org/doi:10.1111/j.1439-0485.2002.tb00006.x>.

675 Carbognin, L., Teatini, P., Tomasin, A., Tosi, L., 2010. Global change and relative sea  
676 level rise at Venice: what impact in term of flooding, *Clim. Dynam.* 35:1039-  
677 1047. <https://doi.org/doi:10.1007/s00382-009-0617-5>.

678 Carbognin, L., Teatini, P., Tosi, L., Strozzi, T., Tomasin, A. (2011). Present relative sea  
679 level rise in the northern Adriatic coastal area. In E. Brugnoli, G. Cavarretta, S.  
680 Mazzola, F. Trincardi, M. Ravaioli, R. Santoleri (Eds.), *Marine Research at CNR-*  
681 *Theme 3 “Coastal and Marine Spatial Planning”* (pp. 1123-1138). CNR-DTA,  
682 Roma, Italy.

683 Chen, B., Gong, H., Li, X., Lei, K., Ke, Y., Duan, G., Zhou, C., 2015. Spatial  
684 correlation between land subsidence and urbanization in Beijing, China, *Nat.*  
685 *Hazards*. 75:2637-2652. <https://doi.org/doi:10.1007/s11069-014-1451-6>.

686 Costantini, M., Ferretti A., Minati Fe., Falco S., Trillo F., Colombo D., Novali F.,  
687 Malvarosa F., Mammone C., Vecchioli F., Rucci A., Fumagalli A., Allievi J.,

688 Ciminelli M., Costabile, S., 2017. Analysis of surface deformations over the  
689 whole Italian territory by interferometric processing of ERS, Envisat and  
690 COSMO-SkyMed radar data. *Remote Sens. Environ.* 202:250-275.  
691 <https://doi.org/doi:10.1016/j.rse.2017.07.017>.

692 Da Lio, C., Tosi, L., Zambon, G., Vianello, A., Baldin, G., Lorenzetti, G., Manfè, G.,  
693 Teatini P., 2013. Long-term groundwater dynamics in the coastal confined  
694 aquifers of Venice (Italy). *Estuar. Coast. Shelf Science.* 135:248-259.  
695 <https://doi.org/doi:10.1016/j.ecss.2013.10.021>.

696 Da Lio, C., Carol, E., Kruse, E., Teatini, P., Tosi, L., 2015. Saltwater contamination in  
697 the managed low-lying farmland of the Venice coast, Italy: An assessment of  
698 vulnerability. *Sci. Total Environ.* 533:356-369.

699 Da Lio, C., Teatini, P., Strozzi, T., Tosi, L., 2018. Understanding land subsidence in salt  
700 marshes of the Venice Lagoon from SAR Interferometry and ground-based  
701 investigations. *Remote Sens. Environ.* 205:56-70.  
702 <https://doi.org/doi:10.1016/j.rse.2017.11.016>.

703 Deverel, S. J., Ingrum, T., Leighton, D., 2016. Present-day oxidative subsidence of  
704 organic soils and mitigation in the Sacramento-San Joaquin Delta, California,  
705 USA. *Hydrogeol. J.* 24:569-586. <https://doi.org/doi:10.1007/s10040-016-1391-1>.

706 Erkens, G., Bucx, T., Dam, R., de Lange, G., Lambert, J., 2015. Sinking coastal cities,  
707 *Proceedings IAHS.* 372:189-198. [https://doi.org/doi:10.5194/piahs-372-189-](https://doi.org/doi:10.5194/piahs-372-189-2015)  
708 2015.

709 Fontana, A., Mozzi, P., Bondesan, A., 2008. Alluvial megafans in the Venetian-Friulian  
710 Plain (north-eastern Italy): Evidence of sedimentary and erosive phases during

711 Late Pleistocene and Holocene. *Quatern. Int.* 189:71-90.  
712 <https://doi.org/doi:10.1016/j.quaint.2007.08.044>.

713 Fontana, A., Mozzi, P., Bondesan, A., 2010. Late Pleistocene evolution of the Venetian-  
714 Friulian Plain. *Rendiconti Fis. Acc. Lincei.* 21:S181-S196.  
715 <https://doi.org/doi:10.1007/s12210-010-0093-1>.

716 Fontolan, G., Pillon, S., Bezzi, A., Villalta, R., Lipizer, M., Triches, A., D'Aiotti, A.,  
717 2012. Human impact and the historical transformation of saltmarshes in the  
718 Marano and Grado Lagoon, northern Adriatic Sea. *Estuar. Coast. Shelf Science.*  
719 113:41-56. <https://doi.org/doi:10.1016/j.ecss.2012.02.007>.

720 Gambolati, G., Putti, M., Teatini, P., Camporese, M., Ferraris, S., Stori, G. G., Nicoletti,  
721 V., Silvestri, S., Rizzetto, F., Tosi, L., 2005. Peat land oxidation enhances  
722 subsidence in the Venice watershed, *Eos Trans. AGU.* 86:217-220.  
723 <https://doi.org/doi:10.1029/2005EO230001>.

724 Higgins, S. A., Overeem, I., Steckler, M. S., Syvitski, J. P. M., Seeber, L., Akhter, S. H.,  
725 2014. InSAR measurements of compaction and subsidence in the Ganges-  
726 Brahmaputra Delta, Bangladesh, *J. Geophys. Res. Earth Surf.* 119:1768-1781.  
727 <https://doi.org/doi:10.1002/2014JF003117>.

728 Luo, Q., Perissin, D., Zhang, Y., Jia, Y., 2014. L- and X-Band multi-temporal InSAR  
729 analysis of Tianjin subsidence. *Remote Sens.* 6:7933-7951.  
730 <https://doi.org/doi:10.3390/rs6097933>.

731 Marani, M., Da Lio, C., D'Alpaos, A., 2013. Vegetation engineers marsh morphology  
732 through multiple competing stable states. *Proc Natl Acad Sci USA.* 110:3259-  
733 3263. <https://doi.org/doi:10.1073/pnas.1218327110>.

734 Marchesini C., 2006. Vertical land movements in the Grado Lagoon (Italy) measured  
735 with various methods. Proceedings of the 3rd IAG/12th FIG symposium, Baden,  
736 May 22-24, 2006.

737 Mauskopf Deliyannis D., 2010. Ravenna in Late Antiquity. Cambridge University  
738 Press.

739 Marocco, R., 1989. Lineamenti geomorfologici della costa e dei fondali del golfo di  
740 Trieste e considerazioni sulla loro evoluzione tardo-quadernaria. *Int. J. Speleol.*  
741 18:87-110.

742 Marocco, R., Melis, R., 2009. Stratigrafia e paleogeografia del “lacus timavi” (Friuli  
743 Venezia Giulia). *Il Quaternario Italian Journal of Quaternary Sciences.* 22:157-  
744 170.

745 Nitti, D.O., De Vitis, L., Bovenga, F., Nutricato, R., Refice, A., Wasowski, J., 2009.  
746 Multi-temporal L-band SAR interferometry confirms C-band spatial patterns of  
747 subsidence in the ancient Wieliczka Salt Mine (Unesco Heritage Site, Poland).  
748 Proceedings of the Fringe 2009 Workshop, Frascati, Italy, 4 December 2009.

749 Rapti-Caputo, D., Bratus, A., Santarato, G., 2009. Strategic groundwater resources in  
750 the Tagliamento River basin (northern Italy): hydrogeological investigation  
751 integrated with geophysical exploration. *Hydrogeol. J.* 17:1393-1409.  
752 <https://doi.org/doi:10.1007/s10040-009-0459-6>.

753 Rebischung, P., Griffiths, J., Ray, J., Schmid, R., Collilieux, X., Garayt, B., 2012.  
754 IGS08: the IGS realization of ITRF2008. *GPS Solut.* 16:483-494.  
755 <https://doi.org/doi:10.1007/s10291-011-0248-2>.

756 Regione Friuli Venezia Giulia. Catalogo Dati Ambientali e Territoriali visualizzazione  
757 cartografica, 2014.

758 <http://irdat.regione.fvg.it/WebGIS/GISViewer.jsp?template=configs:ConfigMAA>  
759 <S/CartografiaGeologica.xml> Accessed January 2018.

760 Rizzetto, F., Tosi, L., 2011. Aptitude of modern salt marshes to counteract relative sea-  
761 level rise, Venice Lagoon (Italy). *Geology*. 39:755-758.  
762 <https://doi.org/doi:10.1130/G31736.1>.

763 Rizzetto, F., Tosi, L., 2012. Rapid response of tidal channel networks to sea-level  
764 variations (Venice Lagoon, Italy). *Global .Plan. Change*. 92-93:191-197.  
765 <https://doi.org/doi:10.1016/j.gloplacha.2012.05.022>.

766 Sestini G., 1996. Land Subsidence and Sea-Level Rise: The Case of the Po Delta  
767 Region, Italy. In J. D. Milliman, B. U. Haq (Eds.), *Sea-Level Rise and Coastal*  
768 *Subsidence. Coastal Systems and Continental Margins* (pp. 235-248). Vol 2.  
769 Springer, Dordrecht.

770 Stefanini, S., Cucchi, F., 1976. Gli acquiferi nel sottosuolo della provincia di Gorizia  
771 (The aquifers in the Gorizia province). *Quaderni Isontini Ricerca Acque*. 28:347-  
772 366.

773 Stefanini, S., Cucchi, F., 1977. Gli acquiferi nel sottosuolo della provincia di Udine  
774 (The aquifers in the Udine province). *Quaderni Isontini Ricerca Acque*. 34:131-  
775 147.

776 Stefanini S., Cucchi F., 1978. Gli acquiferi del sottosuolo della pianura veneta fra i  
777 fiumi Piave e Tagliamento. In: *Indagine sulle falde acquifere profonde della*  
778 *Pianura Padana. Quaderno I.R.S.A.*. 34:287-299.

779 Strozzi, T., Teatini, P., Tosi, L., 2009. TerraSAR-X reveals the impact of the mobile  
780 barrier works on Venice coastland stability. *Remote Sens. Environ.* 113:2682-  
781 2688. <https://doi.org/doi:10.1016/j.rse.2009.08.001>.



782 Strozzi, T., Teatini, P., Tosi, L., Wegmüller, U., Werner, C., 2013. Land subsidence of  
783 natural transitional environments by satellite radar interferometry on artificial  
784 reflectors. *J. Geophys. Res. - Earth Surface.* 118:1177-1191.  
785 <https://doi.org/doi:10.1002/jgrf.20082>.

786 Syvitski, J. P. M., Kettner, A. J., Overeem, I., Hutton, E. W. H., Hannon, M. T.,  
787 Brakenridge, G. R., Day, J., Vörösmarty, C., Saito, Y., Giosan L., Nicholls R. J.,  
788 2009. Sinking deltas due to human activities. *Nature Geoscience.* 2:681-686.  
789 <https://doi.org/doi:10.1038/ngeo629>.

790 Teatini, P., Tosi, L., Strozzi, T., Carbognin, L., Wegmüller, U., Rizzetto, F., 2005.  
791 Mapping regional land displacements in the Venice coastland by an integrated  
792 monitoring system. *Remote Sens. Environ.* 98:403-413.  
793 <https://doi.org/doi:10.1016/j.rse.2005.08.002>.

794 Teatini, P., Strozzi, T., Tosi, L., Wegmüller, U., Werner, C., Carbognin, L., 2007.  
795 Assessing short- and long-time displacements in the Venice coastland by synthetic  
796 aperture radar interferometric point target analysis. *J. Geophys. Res. Earth  
797 Surface.* 112:F01012. <https://doi.org/doi:10.1029/2006JF000656>.

798 Teatini, P., Tosi, L., Strozzi, T., 2011. Quantitative evidence that compaction of  
799 Holocene sediments drives the present land subsidence of the Po Delta, Italy. *J.  
800 Geophys. Res. Solid Earth.* 116:B08407.  
801 <https://doi.org/doi:10.1029/2010JB008122>.

802 Teatini, P., Tosi, L., Strozzi, T., Carbognin, L., Cecconi, G., Rosselli, R., Libardo, S.,  
803 2012. Resolving land subsidence within the Venice Lagoon by persistent scatterer  
804 SAR interferometry. *Phys Chem Earth.* 40-41:72-79.  
805 <https://doi.org/doi:10.1016/j.pce.2010.01.002>.

806 Törnqvist, T. E., Wallace, D. J., Storms, J. E. A., Wallinga, J., van Dam, R. L., Blaauw,  
807 M., Derksen, M. S., Klerks, C. J. W., Meijneken C., Snijders, E. M. A., 2008.  
808 Mississippi Delta subsidence primarily caused by compaction of Holocene strata.  
809 Nature Geoscience. 1:173-176. <https://doi.org/doi:10.1038/ngeo129>.

810 Torresan, S., Critto, A., Rizzi, J., Marcomini, A., 2012. Assessment of coastal  
811 vulnerability to climate change hazards at the regional scale: the case study of the  
812 North Adriatic Sea. Nat. Hazards Earth Syst. Sci. 12:2347-2368.  
813 <https://doi.org/doi:10.5194/nhess-12-2347-2012>.

814 Tosi, L., Teatini, P., Carbognin, L., Frankenfield, J., 2007. A new project to monitor  
815 land subsidence in the northern Venice coastland (Italy). Environ. Geol. 52:889-  
816 898. <https://doi.org/doi:10.1007/s00254-006-0530-8>.

817 Tosi, L., Rizzetto, F., Zecchin, M., Brancolini, G., Baradello, L., 2009.  
818 Morphostratigraphic framework of the Venice lagoon (Italy) by very shallow  
819 water VHRS surveys: evidence of radical changes triggered by human-induced  
820 river diversions. Geophys. Res. Lett. 36: L09406.  
821 <https://doi.org/doi:10.1029/2008GL037136>.

822 Tosi, L., Teatini, P., Strozzi, T., Carbognin, L., Brancolini, G., Rizzetto, F., 2010.  
823 Ground surface dynamics in the northern Adriatic coastland over the last two  
824 decades. Rend. Lincei Sci. Fis. 21:115-129. [https://doi.org/doi:10.1007/s12210-](https://doi.org/doi:10.1007/s12210-010-0084-2)  
825 [010-0084-2](https://doi.org/doi:10.1007/s12210-010-0084-2).

826 Tosi, L., Teatini, P., Bincoletto, L., Simonini, P., Strozzi, T., 2012. Integrating  
827 Geotechnical and Interferometric SAR Measurements for Secondary  
828 Compressibility Characterization of Coastal Soils. Surv. Geophys. 33:907-926.  
829 <https://doi.org/doi:10.1007/s10712-012-9186-y>.

830 Tosi, L., Teatini, P., Strozzi, T., 2013. Natural versus anthropogenic subsidence of  
831 Venice. *Sci. Rep.* 3:2710. <https://doi.org/doi:10.1038/srep02710>.

832 Tosi, L., Strozzi, T., Da Lio, C., Teatini, P., 2015. Regional and local land subsidence at  
833 the Venice coastland by TerraSAR-X PSI. *Proc. IAHS* 372:199-205.  
834 <https://doi.org/doi:10.5194/piahs-372-199-2015>.

835 Tosi, L., Da Lio, C., Strozzi, T., Teatini, P., 2016. Combining L- and X-Band SAR  
836 Interferometry to Assess Ground Displacements in Heterogeneous Coastal  
837 Environments: The Po River Delta and Venice Lagoon, Italy. *Remote Sens.*  
838 8:308. <https://doi.org/doi:10.3390/rs8040308>.

839 Treu F., Analisi dei prelievi da pozzo del Friuli Venezia Giulia, Udine, 1 marzo 2011 -  
840 Giornata di approfondimento sullo stato delle risorse idriche sotterranee in Friuli  
841 Venezia Giulia, Università degli Studi di Trieste, Regione Autonoma del Friuli  
842 Venezia Giulia. [http://www.regione.fvg.it/rafvg/export/sites/default/RAFVG/ambiente-territorio/tutela-ambiente-gestione-risorse-naturali/FOGLIA202/FOGLIA23/allegati/07\\_Treu\\_Francesco.pdf](http://www.regione.fvg.it/rafvg/export/sites/default/RAFVG/ambiente-territorio/tutela-ambiente-gestione-risorse-naturali/FOGLIA202/FOGLIA23/allegati/07_Treu_Francesco.pdf) Accessed  
843 November 2017.

844  
845  
846

847 Trobec, A., Buseti, M., Zgur, F., Baradello, L., Babich, A., Cova, A., Gordini, E.,  
848 Romeo, R., Tomini, I., Poglajen, S., Diviacco, P., Vrabc, M., 2017. Thickness of  
849 marine Holocene sediment in the Gulf of Trieste (Northern Adriatic Sea). *Earth*  
850 *Syst. Sci. Data Discuss.* In review. <https://doi.org/doi:10.5194/essd-2017-135>.

851 USGS Earth Resources Observation and Science (EROS) Center. Terrain model SRTM  
852 1 Arc-Second (2018). <https://earthexplorer.usgs.gov/> Accessed October 2017.

853 Yan, X. X., Gong, S. L., Zeng, Z. Q., 2002. Relationship between building density and  
854 land subsidence in Shanghai urban zone. *Hydrogeol. Eng. Geol.* 6:21-25.

855 Zanferrari, A., Avigliano, R., Fontana, A., Paiero G., 2014. Note illustrative della Carta  
856 Geologica d'Italia alla scala 1: 5.000, 2014, Foglio 086, San Vito al Tagliamento,  
857 pp. 178, APAT, Dip. Difesa del Suolo, Servizio Geologico d'Italia, SystemCart,  
858 Roma.

859 Zini, L., Calligaris, C., Treu, F., Zavagno, E., Iervolino, D., Lippi, F., 2013.  
860 Groundwater sustainability in the Friuli Plain. *AQUA mundi.* 4:41-54.  
861 <https://doi.org/doi:10.4409/Am-058-13-0051>.

862 Zhou, Z., Li, Z., Waldron, S., Tanaka, A., 2016. Monitoring peat subsidence and carbon  
863 emission in Indonesia peatlands using InSAR time series, *IEEE International*  
864 *Geoscience and Remote Sensing Symposium (IGARSS)*, 6797-6798, Beijing.

865 Zoccarato, C., Teatini, P., 2017. Numerical simulations of Holocene salt-marsh  
866 dynamics under the hypothesis of large soil deformations. *Adv. Water Resour.*  
867 110:107-119. <https://doi.org/10.1016/j.advwatres.2017.10.006>.

868

